Available online at www.sciencedirect.com

ScienceDirect

journal homepage: www.elsevier.com/locate/he

# Nickel supported on iron-bearing olivine for $CO_2$ methanation

*Guangyong Wang, Shaoping Xu*, Libing Jiang, Chao Wang*

*State Key Laboratory of Fine Chemicals, Institute of Coal Chemical Engineering, School of Chemical Engineering, Dalian University of Technology, No.2 Linggong Road, Dalian 116024, China*

ARTICLE INFO

*Article history:*
Received 25 January 2016
Received in revised form
2 June 2016
Accepted 4 June 2016
Available online 20 June 2016

*Keywords:*
Methanation
Bimetallic catalyst
Ni–Fe alloy
Olivine

ABSTRACT

Calcined olivine supported nickel catalysts (Ni/olivine) were prepared by incipient wetness method and used for $CO_2$ methanation. To investigate the structure-activity relationships of the catalysts, the structure of the olivine during calcination and that of the Ni/olivine after calcination and reduction were illustrated by means of powder X-ray diffraction, temperature programmed reduction, Mössbauer spectroscopy and BET surface area measurement, and the $CO_2$ methanation were evaluated by using Ni/olivine with different calcination temperatures of the olivine, Ni loadings, calcination and reduction temperatures of the catalyst. It was found that the $FeO_x$ phase formed on the surface of the calcined olivine was extracted from the olivine during its calcination, laying the base for the interaction between the surface $FeO_x$ and the NiO supported. The Ni–Fe alloy as the effective active component was formed on the calcined olivine containing mainly $(Mg_xFe_{1-x})_2$ $SiO_4$ and the thermal induced $FeO_x$ phase, from the reduced NiO and the partially reduced $FeO_x$ during the reduction of the Ni/olivine. The unreduced $FeO_x$ between the active phase Ni–Fe alloy and the olivine body, as the very support of the Ni–Fe alloy, plays an important role in $CO_2$ methanation. With 6 wt.% Ni/olivine prepared under optimized condition as catalyst, at temperature of 400 °C and a $H_2/CO_2$ mole ratio of 6.0 and an hourly space velocity of 11,000 $h^{-1}$, the $CO_2$ methanation achieved 98% $CO_2$ conversion with 99% selectivity to $CH_4$. The Ni/olivine with strong resistance to coke deposition and abrasion could be a promising methanation catalyst, especially for fluidized bed operation.



## Introduction

Synthetic natural gas (SNG) could be produced by catalytic CO/$CO_2$ methanation from syngas of various origins [1–5]. Among variety of methanation catalysts, the supported nickel catalysts are predominant because of their good activity and selectivity and, important for commercial application, relative lower cost [6–9]. The activity and stability of nickel catalysts vary with support materials, promoters and preparation methods [8,10–14]. Specifically, the supports with different specific surface area, thermostability, acidity and basicity, redox property and potential support-metal interactions could greatly influence the catalytic activity of supported catalysts [15–17]. The catalytic performance of nickel supported on $Al_2O_3$, SiC, $SiO_2$, $MgAl_2O_4$, $Ce_xZr_{1-x}O_2$, rice husk ash, etc. has been studied [8,10,11,13,15,16]. It was found that the lattice mismatch between the small $Ni^0$ particles and the support $\gamma$-$Al_2O_3$ leads to the formation of an additional thin interface composed by mixed Ni-$NiC_x$ or $Ni_3C$ in Ni/$\gamma$-$Al_2O_3$, which could result in the

* *Corresponding author.*
E-mail address: huizixu@hotmail.com (S. Xu).
http://dx.doi.org/10.1016/j.ijhydene.2016.06.066

detachment of the Ni-particles from the support during methanation of biomass-derived synthesis gas [18]. Nickel supported on SiC and $MgAl_2O_4$ shows better resistance to coke formation and sintering compared with Ni/$\gamma$-$Al_2O_3$ because of less acidity of the support and moderate interactions between the support and Ni [8,10]. Support matching with the supported metal was suggested to be a key factor in developing supported nickel catalyst with excellent stability [19]. Besides, the activity and stability of the supported catalysts could be improved by the supports via electronical modification and strong metal-support interaction (SMSI) [16,20,21], characterized by reducible supports and reduction treatment under high temperature (typically above 723 K). Based on the reducible nature of $CeO_2$ and $TiO_2$, M/$CeO_2$ and M/$TiO_2$ catalysts exhibiting some sort of SMSI effect were widely studied and used in various applications [22–25]. Catalytic methanation of carbon dioxide by active oxygen material $Ce_xZr_{1-x}O_2$ supported Ni–Co catalyst was reported by Hongwei Zhu et al. [16]. It was suggested that modifications of the structural and redox properties of the support could affect the catalytic performance, in particular, the active oxygen site of $Ce_xZr_{1-x}O_2$ can considerably improve the catalytic activity.

Compared to the traditional Ni-based catalyst, bimetallic $Ni_3Fe$ or NiFe alloy were predicted to be more active and cost-effective than the traditional Ni-based catalyst for methanation by the DFT calculations [6,26,27]. Experimental works focused on this topic were also reported [15,28,29]. A.L. Kustov et al. found that bimetallic catalysts with compositions 25Fe75Ni at low metal loadings and 50Fe50Ni at high metal loadings were efficient for CO methanation [28]. Dharmendra Pandey et al. have systemically investigated the catalytic activities of Ni–Fe bimetallic catalysts for $CO_2$ hydrogenation and they found that Ni and Fe in the ratio of 3:1 supported on $Al_2O_3$, $ZrO_2$, $TiO_2$ and $SiO_2$ showed a higher $CH_4$ yield compared to the supported Ni catalysts [15,29]. Both works suggested that the Ni–Fe alloy formed in the Ni–Fe supported catalysts was effective for CO/$CO_2$ methanation.

Natural olivine with high attrition resistance and good catalytic activity for tar reforming was widely studied in dual bed gasification of biomass [30–34]. It contains $(Mg_xFe_{1-x})_2SiO_4$ as the main phase and small quantities of $MgSiO_3$ and $FeO_x$ species [35–37]. The interactions between supported NiO and $(Mg_xFe_{1-x})_2SiO_4$ might lead to NiO–MgO solid solution formation [36], which was reported to be helpful in enhancing Ni species dispersion and stability of the Ni/olivine [36,38,39]. More importantly, the olivine could be a source of Fe for the supported bimetallic Ni–Fe catalysts. Through high temperature calcination, the iron in the bulk could partly be migrated to the surface of the calcined olivine in the form of $FeO_x$, thus, the redox property of olivine in regards of the iron oxides is controllable. In this way, calcined Fe-bearing olivine could be a potential support behaving in a different way from the inert supports, by providing suitable iron source for the formation of active site (Ni–Fe) and affecting its catalytic activity resulting from the distinctive metal-support relationship as well. Calcined olivine supported nickel (Ni/olivine) has been studied as a cheap steam-reforming nickel-based catalyst [35,36,40] and Ni–Fe alloys were achieved during reduction of the catalyst [36]. However, the calcination temperatures of Ni/olivine were generally as high as 1100 °C–1400 °C to enhance the stability in these works. As a result, the NiO grafted with the support or integrated into olivine structure could hardly be reduced at a temperature well below 910 °C [36,41,42] and predictably has little catalytic activity for $CO_2$ methanation [43]. Ni/olivine or Ni–Fe/olivine prepared for methanation hasn't gained enough attention yet.

In the present work, olivine supported nickel catalyst and its activity for $CO_2$ methanation are reported. Thermal transformation of olivine and Ni/olivine during calcination and reduction has been illustrated by means of powder X-ray diffraction (XRD), temperature programmed reduction (TPR), Mössbauer spectroscopy, X-ray fluorescence (XRF) and BET surface area measurement. The effects of calcination temperature of the olivine, Ni loading, calcination and reduction temperature of the catalyst, and reaction temperature on the catalytic performance of the catalyst have been studied. The structure-activity relationships and the method for catalyst optimization are then proposed.

## Experimental

### *Catalyst preparation*

A natural occurring olivine received from the Chinese city of Yichang was used as catalyst support after calcination at different temperatures (600, 800, 1000 or 1200 °C) for 4.5 h. The Ni/olivine catalysts were prepared by impregnation of the calcined olivine (0.38–0.83 mm) with an aqueous solution of nickel nitrate by the incipient wetness method. Prior to impregnation, the supports were dried at 105 °C for 1 h. The impregnated supports were then dried at room temperature overnight, and heated in air up to different temperatures (350, 600 or 900 °C) with a heating rate of 3 °C/min and kept at the final temperature for 4.5 h. The prepared Ni/olivine catalysts were denoted as x Ni/y-olivine-z, where x (wt.%) represented the mass ratio of Ni to olivine in the finished catalyst, y the calcination temperature (in °C) of olivine and z the calcination temperature of impregnated catalyst. According to the results of XRF analysis, the content of Ni loading fits well within 12% accuracy of that aimed for in the catalyst preparation procedure. As an example, the composition of the 3 Ni/1000-olivine-350 by XRF analysis is given in Table 1. Here 3.28 wt.% NiO in catalyst equals to 2.66 wt.% Ni. A commercial catalyst M-849H provided by Dalian Catalytic Engineering Technology LTD. was used for comparison in this work. As shown in Table 2, it contains 47.33 wt.% NiO and equals to 37.18 wt.% Ni loading.

### *Catalyst characterization*

Specific surface areas measurements of the supports and catalysts were carried out using BET method on the basis of

**Table 1 – Composition of 3 Ni/1000-olivine-350 by XRF analysis (wt.%).**

| MgO | $SiO_2$ | $Fe_2O_3$ | $Al_2O_3$ | CaO | NiO |
|---|---|---|---|---|---|
| 45.87 | 40.65 | 8.28 | 0.96 | 0.96 | 3.28 |

**Table 2 – Composition of M-849H by XRF analysis (wt.%).**

| NiO | $SiO_2$ | $Fe_2O_3$ | $Al_2O_3$ | CaO | MnO | $ZrO_2$ | $Na_2O$ | $SO_3$ | BaO |
|---|---|---|---|---|---|---|---|---|---|
| 47.33 | 0.31 | 0.13 | 36.63 | 0.46 | 8.63 | 5.20 | 0.88 | 0.34 | 0.09 |

$N_2$ physisorption at −196 °C (77 K) on a JW-BK122W apparatus. The chemical composition of the sample was analyzed on a Bruker SRS-3400 XRF analyzer. The crystallite phases in the samples and the structural modifications after calcination and reduction were examined by XRD on a Rigaku D/Max-2400 diffractometer with a nickel-filtered Cu Kα radiation (0.15406 nm) and with a scanning rate of 4° per minute in the 2θ range of 30–55°. Crystallite sizes of the supported Ni or Ni–Fe alloys were determined by the XRD peaks at $2\theta = 44.5°$ using the Debye–Sherrer relation. TPR was conducted on a Quantachrome ChemBET 3000 with a TCD detector. The as-prepared sample (0.2 g) was pretreated at 250 °C in Ar for 2 h prior to TPR measurement, while 5 v/v% $H_2$/Ar with the flow rate of 40 mL/min was used during the TPR experiment. To identify the different forms of iron presented in the sample, the $^{57}$Fe Mössbauer spectrum was recorded at 77 K with a $^{57}$Co source on MFD-500A. The isomeric shifts were determined by comparing with metallic iron standard and the obtained spectrum was fitted with the MossWinn 3.0i XP computer program. Thermal gravimetric analysis (TGA) of the spent catalysts was performed under air flow at a heating rate of 10 °C/min on a DTU-2B thermal balance. The carbon deposited on the catalyst could be determined by the weight loss.

### *Reactivity measurements*

The catalytic performance of the catalysts in $CO_2$ hydrogenation was tested at atmospheric pressure in an electric heated fixed-bed quartz reactor with 8 mm inner diameter. In a typical test, 1 g of the sieved catalyst (0.38–0.83 mm) was placed in the middle of the reactor with a K-type thermocouple placed in the center of catalyst bed to control the reaction temperature. The influence of heat and mass transfer limitations was negligible for $CO_2$ hydrogenation over Ni/olivine with low Ni loading (about 6 wt.%) [8], as indicated in the Supplementary materials. Prior to the activity measurements, all catalysts were reduced in a gas mixture of $H_2/N_2 = 1/4$ for 2 h and then the temperature was lowered to the reaction temperature, typically in the range between 350 and 500 °C. A mixture of $CO_2$ and $H_2$ ($H_2/CO_2 = 3.2$ or 6.0) was then admitted to the reactor at an hourly space velocity of 11,000 $h^{-1}$. The concentrations of CO, $CH_4$ and other gas products were monitored using a GC7890 gas chromatograph equipped with both TCD and FID detectors. The $CO_2$ conversion ($Cco_2 = 1 - \frac{CO_{2\ out}}{CO_{2\ in}}$) and $CH_4$ selectivity ($S_{CH_4} = \frac{CH_{4\ out}}{CO_{2\ in} - CO_{2\ out}}$) were calculated based on the gas phase composition, where $CO_{2\ in}$ was the mole feed rate of $CO_2$, $CO_{2\ out}$ and $CH_{4\ out}$ the mole rate of the effluent $CO_2$ and $CH_4$, respectively. The methanation activity was monitored at least for 1 h in every experiment to ensure a stable catalyst performance. The deviation of the data was within 2% of the reported value indicated by repeat tests.

## Results and discussion

### *Thermal transformation of olivine and Ni/olivine during calcination and reduction*

*Textural properties of olivine and Ni/olivine*

As indicated in Table 3, both the as-received olivine (as-olivine) and the 1000 °C calcined olivine (1000-olivine) show relatively small specific surface area, i.e. 0.83 $m^2/g$ for the as-received [35] and 5.64 $m^2/g$ for the calcined. The obvious increase in surface area after calcination could be attributed to dehydration [37,44] and the formation of extracted iron oxides (indicated by XRD and TPR) during calcination. The surface area of 6 Ni/1000-olivine-350 reaches to 8.48 $m^2/g$, higher than that of the 1000-olivine, indicating that the NiO particles were supported mainly on the surface of 1000-olivine grain, possibly on the thermal induced $FeO_x$ phase, rather than blocking the pores of the support. The specific surface area of the catalyst decreases rapidly with the increase of calcination temperature as a result of phase modifications and increase in the crystallite size of supported NiO species [36].

*Crystallite phases and iron distribution in olivine and Ni/olivine*

The XRD spectra of the calcined olivine and Ni/olivine with different calcination temperatures of the support and different metal loadings are shown in Fig. 1. The Ni/olivine catalysts were reduced in a 20% $H_2/N_2$ mixture at 600 °C for 2 h before XRD tests, while the calcined olivine were examined as prepared. The XRD spectrum of the calcined olivine (Fig. 1a) shows that, with the increase of calcination temperature, the diffraction intensity of $Fe_2O_3$ firstly increases and then decreases, in agreement with the TPR results (Table 6). The intensity of the diffraction lines of enstatite ($MgSiO_3$) and clinoenstatite ($MgSiO_3$) increase steadily up to 1200 °C [45]. Fig. 1b indicated that, the main olivine phase is maintained after calcination and reduction of the catalysts, and a new peak at 44.5° (2θ) appears which can be attributed to the main reflection of the supported metal, i.e. Ni and/or Ni–Fe alloys [36]. The $Fe_2O_3$ peak decrease remarkably after reduction. Additional peaks at 50.9° and 52° could be attributed to the presence of the Ni–Fe alloy [15,29] and Ni [10], respectively. An increase of the Ni–Fe alloy at the expense of Ni could be achieved for Ni/olivine with olivine calcined at moderate temperatures (600–1000 °C). As shown in Fig. 2c, the intensity of the peak at 44.5° increases with the increasing of Ni loadings, while the intensity of the Ni–Fe alloy (50.9°) remains stable. Ni ($2\theta = 52°$) is not detectable in Ni/olivine with 3% Ni-loading and appears in the catalyst with Ni loading of 7.5%,

**Table 3 – Textural properties of as-olivine, calcined olivine and catalyst.**

| Sample | BET surface area ($m^2/g$) |
|---|---|
| as-olivine | 0.83 [35] |
| 1000-olivine | 5.64 |
| 6 Ni/1000-olivine-350 | 8.48 |
| 6 Ni/1000-olivine-600 | 5.21 |
| 6 Ni/1000-olivine-900 | 4.10 |

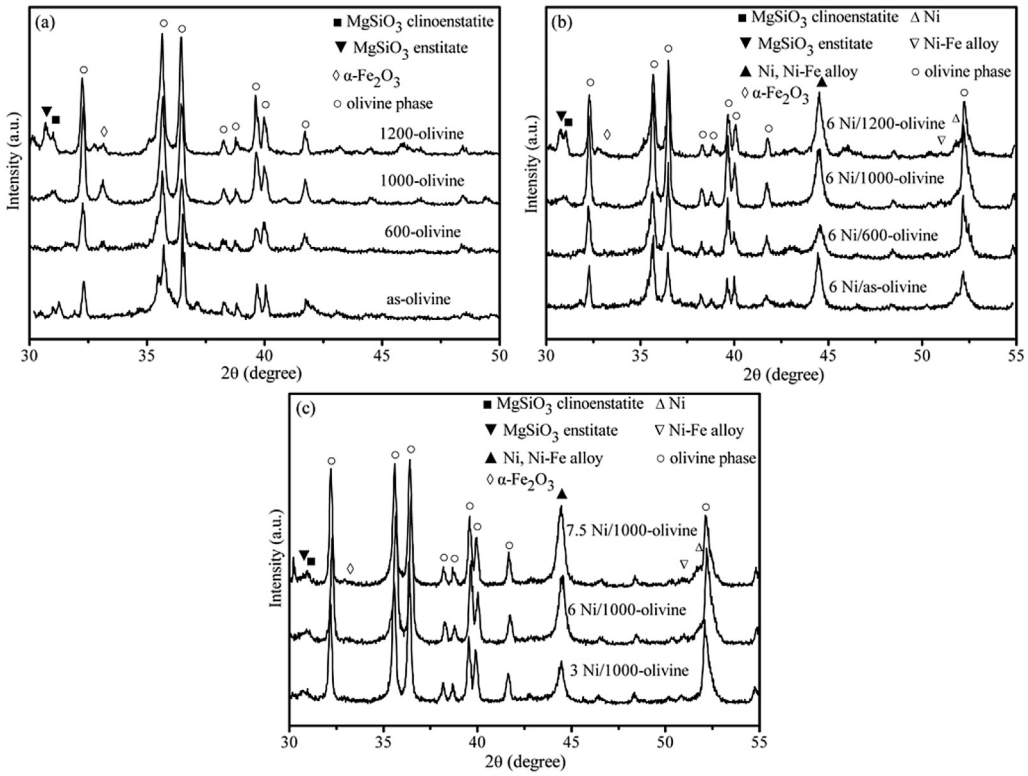


**Fig. 1 – XRD spectra of (a) Olivine calcined at different temperatures, (b) 6 Ni/olivine-350 reduced at 600 °C with different calcination temperatures of the support and (c) Ni/1000-olivine-350 reduced at 600 °C with different Ni loadings.**

indicating a preferred contribution of the supported Ni to the Ni–Fe alloys ($2\theta = 44.5°$) formation.

As displayed in Table 4, the olivines calcined at both 600 °C and 1000 °C as support could lead to the decrease of the crystallite size of Ni or Ni–Fe alloys supported, while that calcined at 1200 °C could not. The metal crystallite sizes of varied Ni loadings on the 1000 °C calcined olivine are almost the same, which ensures a fair comparison of the catalytic performance of the Ni/1000-olivine catalysts with different Ni loadings by using reaction rates normalized to the metal content (mole of $CO_2$ conversion or $CH_4$ production per mole of metal in the catalyst per second) suggested by M.A. Vannice [7] and J.K Nørskov [28]. The comparison is illustrated in Fig. 5b.

The $^{57}$Fe Mőssbauer spectra for the catalyst 6 Ni/1000-olivine-350 reduced at 600 °C are shown in Fig. 2. The parameters of the subspectra, corresponding to the iron distribution in different phases, are given in Table 5. The isomer shift, quadrupole splitting and magnetic field of the sextet S1 ($\delta = 0.37$ mm/s, $\Delta = -0.16$ mm/s and $M = 50.96$ T) correspond to the $Fe^{3+}$ ions presented in $\alpha$-$Fe_2O_3$ oxide (hematite) [30,36]. The hyperfine parameters of S2 could be for $Fe^0$. The isomer shift is slightly positive compared to that of $\alpha$-Fe and the magnetic field is larger than that of iron as a result of the presence of Ni [36], possibly in the form of Ni–Fe alloy [46]. D1

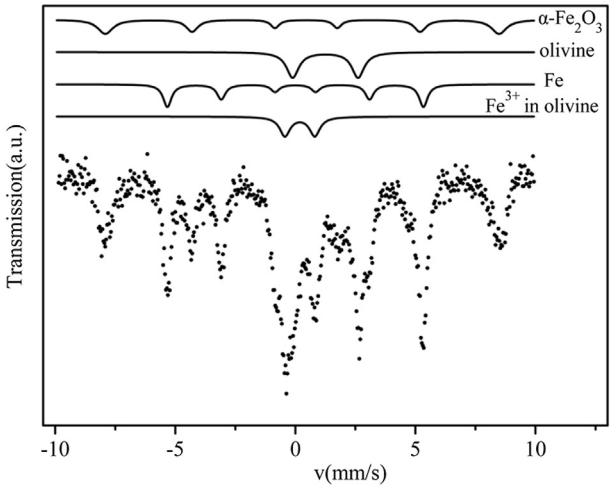


**Fig. 2 – $^{57}$Fe Mőssbauer spectrum at 77 K of the 6 Ni/1000-olivine-350 reduced at 600 °C for 2 h and the subspectra of four components.**

**Table 4 – Metal crystallite size of Ni/olivine-350 reduced at 600 °C with different Ni loadings and different calcination temperatures of olivine.**

| Sample | Metal crystallite size (nm) |
|---|---|
| 3 Ni/1000-olivine | 28 |
| 7.5 Ni/1000-olivine | 28 |
| 6 Ni/as-olivine | 35 |
| 6 Ni/600-olivine | 25 |
| 6 Ni/1000-olivine | 27 |
| 6 Ni/1200-olivine | 35 |

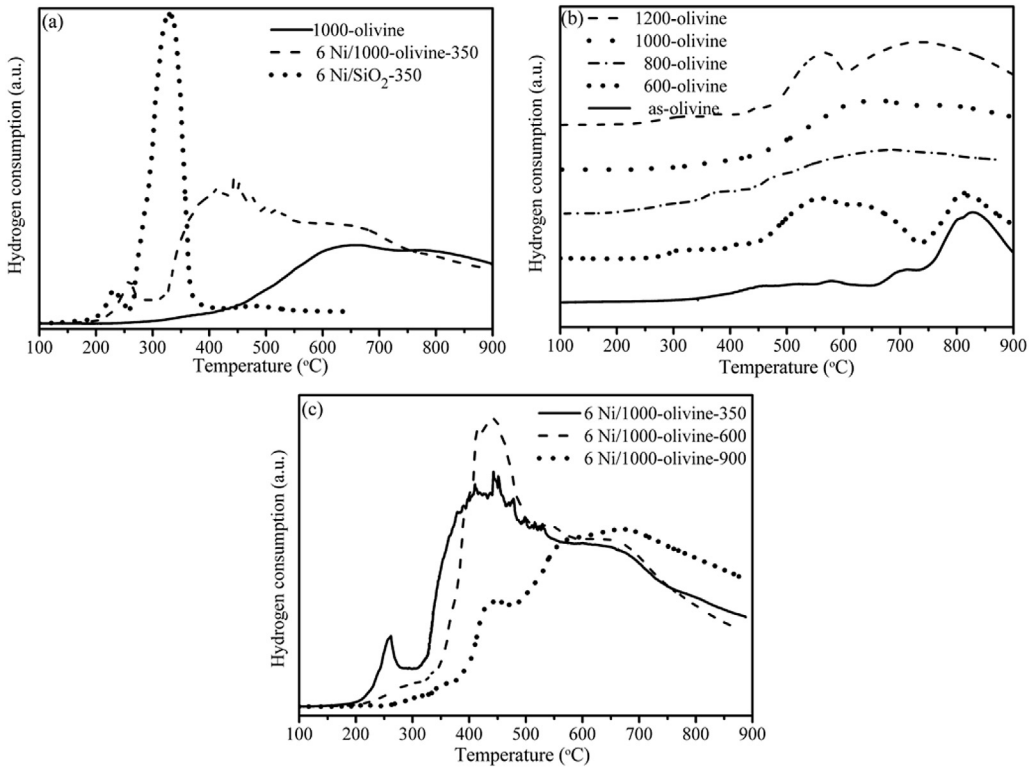


**Fig. 3 – TPR profiles of (a) the supported nickel catalysts, (b) olivine calcined at different temperatures and (c) 6 Ni/1000-olivine catalysts calcined at different temperatures.**

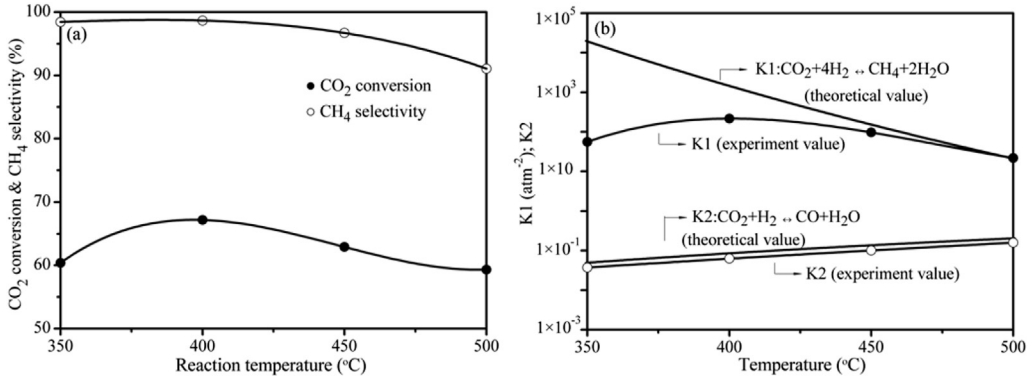


**Fig. 4 – The temperature dependences of (a) $CO_2$ conversion and $CH_4$ selectivity over 6 Ni/1000-olivine-350 reduced at 500 °C and (b) reaction equilibrium constants. GHSV = 11,000 $h^{-1}$, $H_2/CO_2$ = 3.2.**

presented in the Mössbauer spectra with an isomer shift of 1.25 mm/s and quadrupole splitting of 2.72 mm/s attributes to $Fe^{2+}$ ions in the olivine structure [30,36,47]. The doublet D2 with $\delta = 0.19$ mm/s and $\Delta = 1.25$ mm/s can be assigned to $Fe^{3+}$ in olivine, probably at M2 [47–50]. Mössbauer spectroscopy confirms 28.9% of total iron in the 1000 °C calcined olivine has been reduced to $Fe^0$ at 600 °C, and Ni/(Ni + Fe) mole ratio in Ni/1000-olivine is thus determined by the results of XRF and Mössbauer spectroscopy analysis.

*Interactions between different phases in olivine and Ni/olivine*

As shown in the $H_2$-TPR profiles in Fig. 3a, the reduction peak of NiO supported on 1000-olivine moves to higher temperature compared to that on $SiO_2$, indicating that there was a stronger interaction between NiO and the 1000 °C calcined olivine than that between NiO and $SiO_2$.

$H_2$-TPR profiles of the as-received olivine and the olivine calcined at different temperatures between 600 and 1200 °C are shown in Fig. 3b. The as-received olivine is only slightly reduced before 750 °C, corresponding to the little free iron oxides as observed with XRD. While the intensity of the reduction peak increases greatly after calcination, mainly contributed by the reduction of the thermal induced iron oxides as illustrated in Fig. 1a and b. It could be conclude that iron was extracted from the olivine structure during calcination [45] and the $FeO_x$ phase was formed on the surface of the

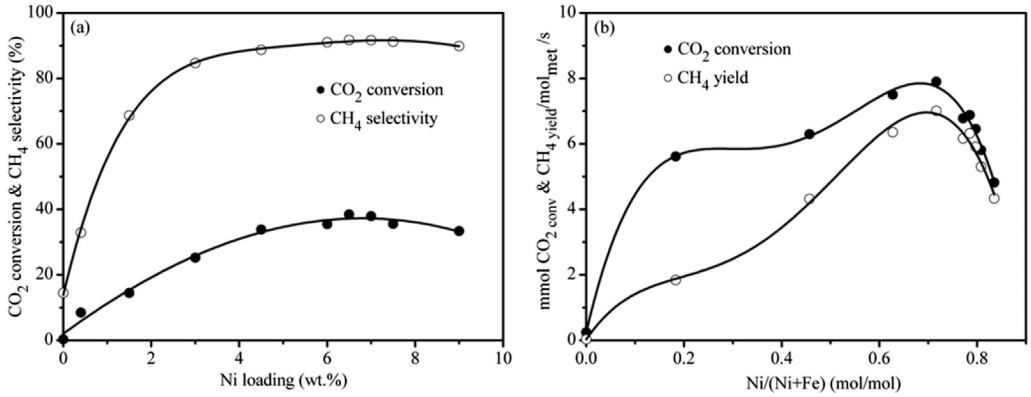


**Fig. 5 – $CO_2$ conversion, $CH_4$ selectivity and rates of $CO_2$ hydrogenation over Ni/1000-olivine-350 reduced at 600 °C as a function of Ni loading and Ni/(Ni + Fe) at 350 °C. GHSV = 11,000 $h^{-1}$, $H_2/CO_2$ = 3.2.**

**Table 5 – Mössbauer parameters of components presented in 6 Ni/1000-olivine-350 reduced at 600 °C.**

| | δ (mm/s) | Δ (mm/s) | M (T) | R (%) |
|---|---|---|---|---|
| D 2 ($Fe^{3+}$) | 0.19 | 1.25 | _ | 15.3 |
| S 2 ($Fe^0$) | 0.0003 | 0.0016 | 33.13 | 28.9 |
| D 1 (olivine) | 1.25 | 2.72 | _ | 24.0 |
| S 1 ($Fe^{3+}$) | 0.37 | −0.16 | 50.96 | 31.8 |

δ, isomer shift related to metallic iron; Δ, quadrupole splitting; M, magnetic field; R, relative area.

calcined olivine as indicated above. Table 6 shows the percentage of reduced iron (from the surface $FeO_x$) in the as-received and calcined olivine after reduction at 600 °C (or at 500 and 650 °C) for 2 h, which is calculated from the hydrogen consumption during TPR experiments (1 mol $H_2$ could reduce 2/3 mol $Fe_2O_3$ which is the main form of reducible iron in the calcined olivine) [30]. The amount of reducible iron increases with the calcination temperature rising up to 800 °C. However, a slight reversal trend occurs when the calcination temperature continues to increase, which could be attributed to the reintegration of the extracted iron into the olivine framework at higher temperature [45,51]. It is noted that reducible iron content increases again after calcination at 1200 °C, which might result from the reaction between the amorphous silica around iron oxide particles and olivine to form $MgSiO_3$, facilitating the access of $H_2$, and thus more iron oxides could be reduced [45]. The formation of $MgSiO_3$ has been confirmed by the increase of the intensity of $MgSiO_3$ in the XRD spectrum. The weight percents of metallic iron after reduction of the calcined olivine at different temperatures are also shown in Table 6, indicating that the amount of reducible iron increases with the increase of reduction temperature.

**Table 6 – Metallic iron on olivine with different calcination and reduction temperatures.**

| Calcination temperature (°C) | Reduction temperature (°C) | $Fe^0$ (wt.%) |
|---|---|---|
| as-received | 600 | 1.3 |
| 600 | 600 | 2.2 |
| 800 | 600 | 2.7 |
| 1000 | 600 | 2.4 |
| 1200 | 600 | 2.6 |
| 1000 | 500 | 1.9 |
| 1000 | 650 | 2.5 |

The TPR profiles for Ni/olivine catalysts calcined at different temperatures are shown in Fig. 3c, in which a high peak of hydrogen consumption between 350 °C and 550 °C is observed, attributing to the reduction of nickel species and the extracted iron oxides resulting from olivine calcination. For the catalyst calcined at 350 °C, a small hydrogen consumption at 260 °C is noticed, indicating that part of the supported nickel was just deposited on the olivine surface in a weak interaction type, possibly in the form of highly dispersed nickel species [36,52]. For the catalyst after 900 °C calcination, the major hydrogen consumption zone moves to higher temperature, which results from the formation of NiO–MgO solid-solution phase and grafted NiO [10,36,41].

As mentioned above, an optimal quantity of reducible iron and Ni/Fe ratio could be achieved in Ni/olivine with the adjustment of the calcination temperature of the support and the calcination and reduction temperature of the catalyst.

### *$CO_2$ methanation over Ni/olivine catalysts*

#### *Effect of the reaction temperature*

The temperature dependences of $CO_2$ conversion and $CH_4$ selectivity over 6 Ni/1000-olivine-350 reduced at 500 °C are shown in Fig. 4a. $CO_2$ conversion increases with the reaction temperature rising up to 400 °C and then decreases. The $CH_4$ selectivity remains constant between 350 and 400 °C, followed by rapid decrease in selectivity with increasing reaction temperature. The results are in the level of the reported highly efficient catalysts [11,17,53,54] for $CO_2$ methanation at atmospheric pressure. From the viewpoint of thermodynamics, as shown in Fig. 4b, the $CO_2$ methanation reaction approaches to chemical equilibrium at reaction temperature higher than 450 °C while the reverse water gas shift reaction nears to chemical equilibrium in a wide range of 350–500 °C. Thus, the chemical equilibrium restricted the methanation at higher reaction temperature [14,55]. In addition, a higher reaction temperature promoted side reactions, leading to the lower

$CH_4$ selectivity. Therefore, 400 °C is the optimum reaction temperature for hydrogenation of $CO_2$ over the provided catalysts. Notably, 350 °C should be recommended as the appropriate reaction temperature to evaluate the catalytic activities of Ni/olivine with different Ni/(Ni + Fe) mole ratio, at which the methanation is far from chemical reaction equilibrium and is controlled by dynamic factor.

*Effect of Ni loading and Ni/(Ni + Fe) mole ratio*

In Fig. 5, the catalytic activities of the Ni/olivine catalysts for $CO_2$ methanation at 350 °C are shown as a function of Ni loading and Ni/(Ni + Fe) mole ratio. The $CO_2$ conversion and $CH_4$ selectivity increase with the Ni loading up to 6.5%, and then remain stable. The maximum rate of $CO_2$ hydrogenation over Ni/olivine with different Ni/(Ni + Fe) ratio is found to be around 0.75. The results conforms the experimental $CO/CO_2$ methanation data [15,28,29]. It has been suggested that $Ni_3Fe$ alloy formed in the supported Ni–Fe catalysts was effective for $CO/CO_2$ methanation [15,28,29], although other irregular Ni–Fe alloys with the composition NiFe, $Ni_3Fe_2$ and $Ni_2Fe$ have also been reported [28]. In addition, The literature computational screening results [6,26,56] revealed that the $Ni_3Fe$ alloy (Ni/(Ni + Fe) ratio = 0.75) was the most active component among Fe, Ni and Ni–Fe alloys with other Ni/Fe ratios. It appears that the Ni–Fe alloy formed indicated by XRD, such as $Ni_3Fe$, improves the catalytic activity of Ni/olivine with optimized composition.

*Effect of the olivine calcination temperature*

The calcination temperature of the support can greatly affect the catalyst activity as shown in Fig. 6. Catalyst with the support calcined at moderate temperature has a better catalytic performance than those with either the as-received olivine (corresponding to the calcination temperature the Ni/olivine underwent, i.e. 350 °C) or 1200-olivine as support, resulting from the smaller metal particle sizes (Table 4) and the Ni–Fe alloy formation. As mentioned above, NiO particles were supported mainly on the thermal induced $FeO_x$ phase on the surface of 1000-olivine grain. The amount of the thermal induced $FeO_x$ increased with the calcination temperature rising up to 800 °C and then decreased due to the reintegration of the extracted iron into the olivine framework at higher temperature. Olivine calcination at 600–1000 °C gained more $FeO_x$ compared with the as-received olivine and 1200-olivine and thus could provide much more surface to improve the dispersion of the supported NiO particles, which may also promote the formation of the Ni–Fe alloy indicated by XRD as mentioned above.

*Effect of the catalyst reduction temperature*

The effect of reduction temperature on catalyst activity for $CO_2$ methanation at 400 °C was studied based on the catalyst 6 Ni/1000-olivine-350 and the result is shown in Fig. 7. The $CO_2$ conversion and $CH_4$ selectivity decrease with the reduction temperature increasing from 500 to 650 °C. As indicated in Table 6, more iron in olivine would be reduced at higher reduction temperature, which could alter the Ni/(Ni + Fe) ratio of Ni/olivine and the amount of the active metal support $FeO_x$ (indicated by TPR and Mössbauer spectra) remained. The Ni/(Ni + Fe) ratio of the catalyst reduced at 650 °C is closer to the optimal value compared with that reduced at the lower temperatures while its $CO_2$ conversion and $CH_4$ selectivity are worse, indicating that the Ni/(Ni + Fe) ratio of the catalyst could not be the only decisive factor of its catalytic activity. It has been suggested that the unreduced iron oxides supply adsorbed carbonate species for the $CO_2$ hydrogenation to occur more efficiently [29]. In addition, the reducible support were reported to greatly affect the activity and stability of supported catalysts by electronical modification and SMSI [16,20,21]. As shown in Fig. 7, the catalytic performance of the catalyst is related to the reduction temperature, which could determine the Ni/(Ni + Fe) ratio and the amount of $FeO_x$ remained as well. More $FeO_x$ would be remained at lower reduction temperature. It is reasonable to deduced that the unreduced $FeO_x$ between the active phase Ni–Fe alloy and the olivine body, as the support of the Ni–Fe alloy, plays an important role in $CO_2$ methanation, though further work is needed to clarify the mechanism of the promotion effect of the $FeO_x$.

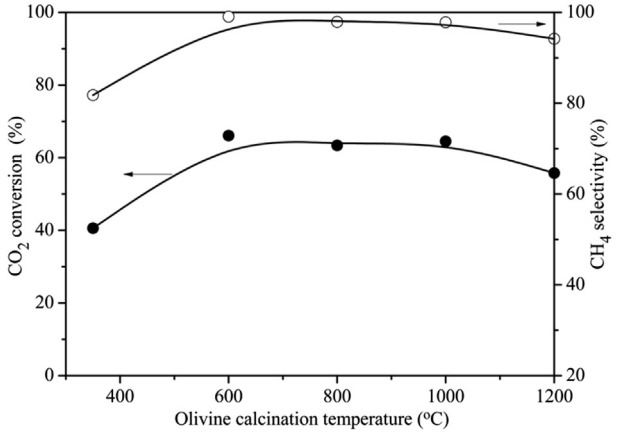


**Fig. 6 – Effect of the calcination temperature of the support on $CO_2$ conversion and $CH_4$ selectivity for $CO_2$ hydrogenation over 6 Ni/olivine-350 reduced at 600 °C. GHSV = 11,000 $h^{-1}$, $H_2/CO_2$ = 3.2, T = 400 °C.**

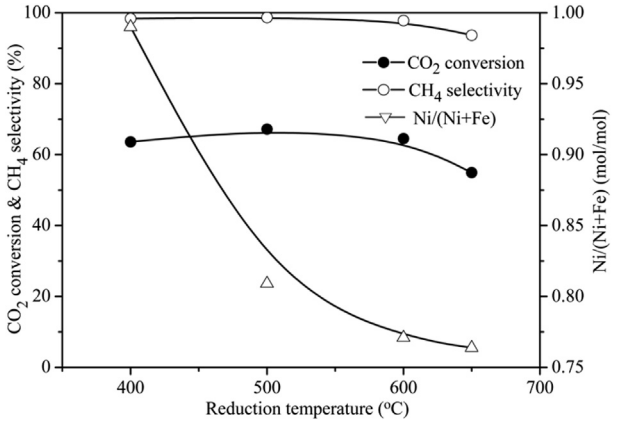


**Fig. 7 – $CO_2$ conversion and $CH_4$ selectivity of $CO_2$ hydrogenation at 400 °C over 6 Ni/1000-olivine-350 of varied reduction temperature and Ni/(Ni + Fe) mole ratio. GHSV = 11,000 $h^{-1}$, $H_2/CO_2$ = 3.2.**

*Effect of the catalyst calcination temperature*

Fig. 8 displays the effect of calcination temperature of the catalyst on its catalytic performance for $CO_2$ methanation at 400 °C. With the increase of the calcination temperature, the $CO_2$ conversion decreases rapidly and the $CH_4$ selectivity drops slightly. The decrease of BET surface area (as shown in Table 3) and the loss of exposed active sites by the formation of grafted NiO and NiO–MgO solid solution [36,57] which is difficult to reduce under methanation conditions, as shown by TPR (Fig. 3c), deteriorate the catalytic activities. The TPR results also reveal that the peak of highly dispersed Ni species (at 260 °C in Fig. 3c), which is active for $CO_2$ methanation [52], disappears at calcination temperatures higher than 600 °C. Furthermore, the thermally induced sintering could result in a decrease of surface area of the Ni particles and a loss of catalyst activity [58].

*Comparison of the Ni/olivine with a commercial catalyst*

Comparison of the catalytic behavior between 6 Ni/1000-olivine-350 and the commercial catalyst M-849H are shown in Table 7 and Fig. 9. The catalytic activity of 6 Ni/1000-olivine-350 is comparable to that of M-849H with a Ni loading as high as 37 wt.%. Due to the formation of the Ni–Fe alloy and the active support, Ni/olivine with low Ni loading obtained a high methanation efficiency. At methanation temperature of 400 °C and $H_2/CO_2$ of 6.0, the Ni/olivine reduced at 500 °C, achieves 98% $CO_2$ conversion with 99% selectivity to $CH_4$. The results also indicate that 6 wt.% Ni/olivine catalyst can be a potential catalyst for $CH_4$ production from $CO_2$ hydrogenation.

The TGA profiles of both the 6 wt.% Ni/olivine and the commercial catalyst, after methanation at 400 °C for 5 h in a mixture of $CO_2$ and $H_2$ ($H_2/CO_2 = 3.2$) at an hourly space velocity of 11,000 $h^{-1}$, are shown in Fig. 9. The curves can be divided into two stages, the first stage, below 300 °C, related to the removal of moisture and volatile materials absorbed on the catalyst [59], while the second stage, above 300 °C, corresponding to the burning of carbon species and oxidation of the supported metal on the catalyst [8]. The distinct weight increase of the commercial catalyst between 250 and 400 °C is due to the metal oxidation overwhelming the burning of carbon species, while an opposite tendency appears at higher temperature. The potential oxidation peak of the metallic nickel and iron in Ni/olivine (corresponding to the reduction peak at 450 °C in Fig. 3) disappears under the effect of the oxidation peak of carbon [8]. The small weight loss of the Ni/olivine catalyst indicates its strong resistance to coke deposition compared with the commercial catalyst. The remarkable carbon-deposition resistance may result from the formation of the Ni–Fe alloy [36] and the SMSI state which might originate from the strong interaction between the Ni–Fe alloy and the partially reduced $FeO_x$, and the strong bonding of the Ni–Fe alloy to the support resulting from the formation of small amounts of NiO–MgO solid-solution phase [10,36].

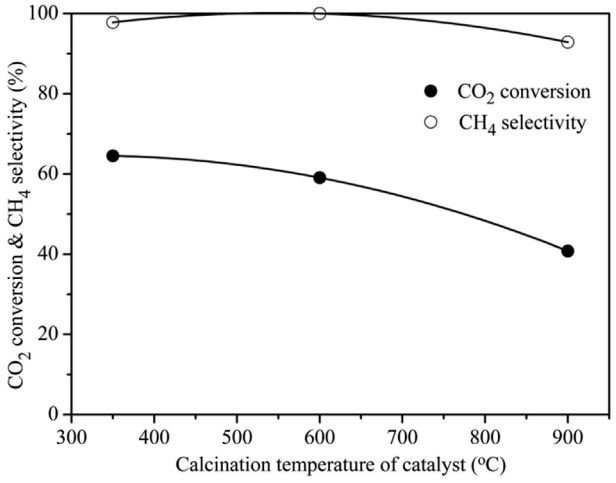


**Fig. 8 – Effect of the calcination temperature of catalyst on $CO_2$ conversion and $CH_4$ selectivity for $CO_2$ hydrogenation over 6 Ni/1000-olivine reduced at 600 °C. GHSV = 11,000 $h^{-1}$, $H_2/CO_2 = 3.2$, T = 400 °C.**

**Table 7 – Comparison of $CO_2$ conversion and $CH_4$ selectivity for $CO_2$ hydrogenation over 6 Ni/1000-olivine-350 reduced at 500 °C and a commercial catalyst with $H_2/CO_2 = 3.2$ and 6.0, GHSV = 11,000 $h^{-1}$, T = 400 °C.**

| Catalyst | $H_2/CO_2$ mole ratio | $CO_2$ conversion/% | $CH_4$ selectivity/% |
|---|---|---|---|
| Ni/olivine | 3.2 | 67.2 | 98.7 |
| | 6.0 | 98.4 | 99.9 |
| M-849H | 3.2 | 67.1 | 98.8 |
| | 6.0 | 98.2 | 99.9 |

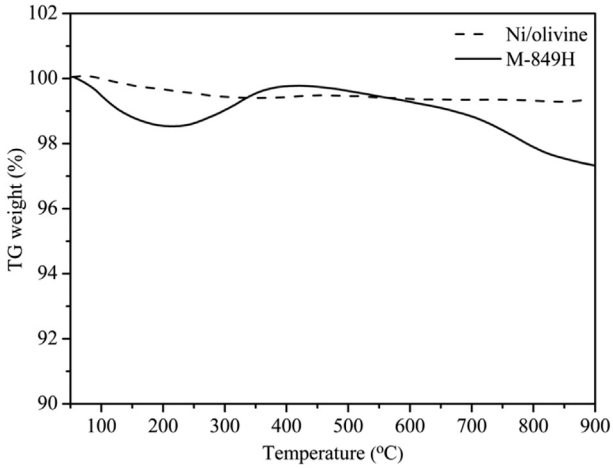


**Fig. 9 – TGA curves of the spent 6 Ni/1000-olivine-350 and a commercial catalyst.**

## Conclusions

Thermal transformation of olivine and Ni/olivine during calcination and reduction, and its influence on the catalytic performance of Ni/olivine in $CO_2$ methanation were studied.

The thermal transformation of olivine during calcination and the following reduction of the catalyst determines the crystallite size and species of the active phases, Ni/(Ni + Fe) ratio and redox property of the support. During the calcination of olivine, $FeO_x$ were extracted from the olivine and formed on its surface. The amount of the thermal induced $FeO_x$ increased with the calcination temperature rising up to 800 °C

and then decreased. The olivine calcined at moderate temperature could improve the dispersion of the metal supported due to more $FeO_x$ extracted which would act as the support of the supported NiO and provide more surface area.

The calcination of olivine laid the base for the interaction between the surface $FeO_x$ and the NiO supported during the catalyst reduction. The thermal induced iron transfer during the reduction could affect the Ni/(Ni + Fe) ratio as well as the amount of the $FeO_x$. More iron in the $FeO_x$ could be reduced at higher reduction temperature, thus the Ni/(Ni + Fe) ratio of Ni/olivine and the amount of the remained $FeO_x$ decreased. The catalyst with around 0.75Ni/(Ni + Fe) (mol/mol) gained the maximum $CO_2$ methanation activity, which could result from the formation of the Ni–Fe alloy. The unreduced $FeO_x$ between the active phase Ni–Fe alloy and the olivine body, as the very support of the Ni–Fe alloy, plays an important role in $CO_2$ methanation. The balance between the Ni–Fe alloy and the remained $FeO_x$ is crucial for catalyst optimization. Nevertheless, the role of the $FeO_x$ should be further elucidated.

The catalytic activity of 6 Ni/1000-olivine-350 after 500 °C reduction was comparable to that of commercial catalyst. At temperature of 400 °C and a $H_2/CO_2$ mole ratio of 6.0 and an hourly space velocity of 11,000 $h^{-1}$, the $CO_2$ methanation achieved 98% $CO_2$ conversion with 99% selectivity to $CH_4$. Ni/olivine with low Ni loading, simple preparation and high attrition resistance could be a promising methanation catalyst, especially for fluidized bed methanation.

## Acknowledgments

The authors gratefully acknowledge the financial support for this work provided by the Natural Science Foundation of China (No. 50776013) and the National High Technology Research and Development Program of China (No. 2008AA05Z407).

## Appendix A. Supplementary data

Supplementary data related to this article can be found at http://dx.doi.org/10.1016/j.ijhydene.2016.06.066.

## REFERENCES

[1] Gröbl T, Walter H, Haider M. Biomass steam gasification for production of SNG-process design and sensitivity analysis. Appl Energy 2012;97:451–61.
[2] Nanou P, van Swaaij WP, Kersten SR, van Rossum G. Evaluation of catalytic effects in gasification of biomass at intermediate temperature and pressure. II. Process performance analysis. Energy & Fuels 2011;25:4085–94.
[3] Zwart RW, Boerrigter H. High efficiency co-production of synthetic natural gas (SNG) and Fischer-Tropsch (FT) transportation fuels from biomass. Energy & Fuels 2005;19:591–7.
[4] Jeon S, Park C, Hackett C, Norbeck J. Characteristics of steam hydrogasification of wood using a micro-batch reactor. Fuel 2007;86:2817–23.
[5] Wei L, Xu S, Zhang L, Liu C, Zhu H, Liu S. Steam gasification of biomass for hydrogen-rich gas in a free-fall reactor. Int J Hydrogen Energy 2007;32:24–31.
[6] Andersson MP, Bligaard T, Kustov A, Larsen KE, Greeley J, Johannessen T, et al. Toward computational screening in heterogeneous catalysis: pareto-optimal methanation catalysts. J Catal 2006;239:501–6.
[7] Vannice M. The catalytic synthesis of hydrocarbons from $H_2$CO mixtures over the Group VIII metals: V. The catalytic behavior of silica-supported metals. J Catal 1977;50:228–36.
[8] Zhang G, Sun T, Peng J, Wang S, Wang S. A comparison of Ni/SiC and Ni/$Al_2O_3$ catalyzed total methanation for production of synthetic natural gas. Appl Catal A-General 2013;462:75–81.
[9] Gao Z, Cui L, Ma H. Selective methanation of CO over Ni/$Al_2O_3$ catalyst: effects of preparation method and Ru addition. Int J Hydrogen Energy 2016;41:5484–93.
[10] Lebarbier VM, Dagle RA, Kovarik L, Albrecht KO, Li X, Li L, et al. Sorption-enhanced synthetic natural gas (SNG) production from syngas: a novel process combining CO methanation, water-gas shift, and $CO_2$ capture. Appl Catal B Environ 2014;144:223–32.
[11] Chang F-W, Kuo M-S, Tsay M-T, Hsieh M-C. Hydrogenation of $CO_2$ over nickel catalysts on rice husk ash-alumina prepared by incipient wetness impregnation. Appl Catal A General 2003;247:309–20.
[12] Satthawong R, Koizumi N, Song C, Prasassarakich P. Comparative study on $CO_2$ hydrogenation to higher hydrocarbons over Fe-based bimetallic catalysts. Top Catal 2014;57:588–94.
[13] Yan X, Liu Y, Zhao B, Wang Z, Wang Y, Liu C. Methanation over Ni/$SiO_2$: effect of the catalyst preparation methodologies. Int J Hydrogen Energy 2013;38:2283–91.
[14] Lu H, Yang X, Gao G, Wang K, Shi Q, Wang J, et al. Mesoporous zirconia-modified clays supported nickel catalysts for CO and $CO_2$ methanation. Int J Hydrogen Energy 2014;39:18894–907.
[15] Pandey D, Deo G. Effect of support on the catalytic activity of supported Ni-Fe catalysts for the $CO_2$ methanation reaction. J Industrial Eng Chem 2016;33:99–107.
[16] Zhu H, Razzaq R, Li C, Muhmmad Y, Zhang S. Catalytic methanation of carbon dioxide by active oxygen material $Ce_xZr_{1-x}O_2$ supported Ni Co bimetallic nanocatalysts. AIChE J 2013;59:2567–76.
[17] Wang W, Chu W, Wang N, Yang W, Jiang C. Mesoporous nickel catalyst supported on multi-walled carbon nanotubes for carbon dioxide methanation. Int J Hydrogen Energy 2016;41:967–75.
[18] Czekaj I, Loviat F, Raimondi F, Wambach J, Biollaz S, Wokaun A. Characterization of surface processes at the Ni-based catalyst during the methanation of biomass-derived synthesis gas: X-ray photoelectron spectroscopy (XPS). Appl Catal A General 2007;329:68–78.
[19] Cui D, Liu J, Yu J, Yue J, Su F, Xu G. Necessity of moderate metal-support interaction in Ni/$Al_2O_3$ for syngas methanation at high temperatures. RSC Adv 2015;5:10187–96.
[20] Farmer JA, Campbell CT. Ceria maintains smaller metal catalyst particles by strong metal-support bonding. Science 2010;329:933–6.
[21] Shiju NR. The role of metal-support bonding in controlling the particle size of ceria-supported transition metal catalysts. ChemCatChem 2011;3:112–4.
[22] Bernal S, Botana F, Calvino J, Lopez C, Pérez-Omil J, Rodriguez-Izquierdo J. High-resolution electron microscopy investigation of metal-support interactions in Rh/$TiO_2$. J Chem Soc Faraday Trans 1996;92:2799–809.

[23] Beckers J, Rothenberg G. Sustainable selective oxidations using ceria-based materials. Green Chem 2010;12:939–48.
[24] Bernal S, Calvino J, Cauqui M, Gatica J, Larese C, Omil JP, et al. Some recent results on metal/support interaction effects in NM/$CeO_2$ (NM: noble metal) catalysts. Catal Today 1999;50:175–206.
[25] Razzaq R, Li C, Amin N, Zhang S, Suzuki K. Co-methanation of carbon oxides over nickel-based $Ce_xZr_{1-x}O_2$ catalysts. Energy & Fuels 2013;27:6955–61.
[26] Nørskov JK, Bligaard T, Rossmeisl J, Christensen CH. Towards the computational design of solid catalysts. Nat Chem 2009;1:37–46.
[27] Wang Y, Su Y, Zhu M, Kang L. Mechanism of CO methanation on the $Ni_4/\gamma$-$Al_2O_3$ and $Ni_3$ Fe/$\gamma$-$Al_2O_3$ catalysts: a density functional theory study. Int J Hydrogen Energy 2015;40:8864–76.
[28] Kustov A, Frey AM, Larsen KE, Johannessen T, Nørskov JK, Christensen CH. CO methanation over supported bimetallic Ni-Fe catalysts: from computational studies towards catalyst optimization. Appl Catal A General 2007;320:98–104.
[29] Pandey D, Deo G. Promotional effects in alumina and silica supported bimetallic Ni-Fe catalysts during $CO_2$ hydrogenation. J Mol Catal A Chem 2014;382:23–30.
[30] Virginie M, Adánez J, Courson C, De Diego L, García-Labiano F, Niznansky D, et al. Effect of Fe-olivine on the tar content during biomass gasification in a dual fluidized bed. Appl Catal B Environ 2012;121:214–22.
[31] Wilk V, Hofbauer H. Co-gasification of plastics and biomass in a dual fluidized-bed steam gasifier: possible interactions of fuels. Energy & Fuels 2013;27:3261–73.
[32] Zou W, Song C, Xu S, Lu C, Tursun Y. Biomass gasification in an external circulating countercurrent moving bed gasifier. Fuel 2013;112:635–40.
[33] Fredriksson HO, Lancee RJ, Thüne PC, Veringa HJ, Niemantsverdriet JH. Olivine as tar removal catalyst in biomass gasification: catalyst dynamics under model conditions. Appl Catal B Environ 2013;130:168–77.
[34] Abdoulmoumine N, Adhikari S, Kulkarni A, Chattanathan S. A review on biomass gasification syngas cleanup. Appl Energy 2015;155:294–307.
[35] Yang X, Xu S, Xu H, Liu X, Liu C. Nickel supported on modified olivine catalysts for steam reforming of biomass gasification tar. Catal Commun 2010;11:383–6.
[36] Swierczynski D, Courson C, Bedel L, Kiennemann A, Guille J. Characterization of Ni-Fe/MgO/olivine catalyst for fluidized bed steam gasification of biomass. Chem Mater 2006;18:4025–32.
[37] Kuhn JN, Zhao Z, Felix LG, Slimane RB, Choi CW, Ozkan US. Olivine catalysts for methane-and tar-steam reforming. Appl Catal B Environ 2008;81:14–26.
[38] Li Y, Lu G, Ma J. Highly active and stable nano NiO-MgO catalyst encapsulated by silica with a core-shell structure for $CO_2$ methanation. RSC Adv 2014;4:17420–8.
[39] Guo M, Lu G. The effect of impregnation strategy on structural characters and $CO_2$ methanation properties over MgO modified Ni/$SiO_2$ catalysts. Catal Commun 2014;54:55–60.
[40] Pfeifer C, Rauch R, Hofbauer H. In-bed catalytic tar reduction in a dual fluidized bed biomass steam gasifier. Industrial Eng Chem Res 2004;43:1634–40.
[41] Pfeifer C, Rauch R, Hofbauer H, Świerczyński D, Courson C, Kiennemann A. Hydrogen-rich gas production with a Ni-catalyst in a dual fluidized bed biomass gasifier. Sci Therm Chem Biomass Convers 2004:677–90.
[42] Zhao Z, Lakshminarayanan N, Swartz SL, Arkenberg GB, Felix LG, Slimane RB, et al. Characterization of olivine-supported nickel silicate as potential catalysts for tar removal from biomass gasification. Appl Catal A General 2015;489:42–50.
[43] Zhao Z, Kuhn JN, Felix LG, Slimane RB, Choi CW, Ozkan US. Thermally impregnated Ni-olivine catalysts for tar removal by steam reforming in biomass gasifiers. Industrial Eng Chem Res 2008;47:717–23.
[44] Yang X. Olivine-supported nickel catalysts for steam reforming of biomass tar. Thesis, Dalian: Dalian University of Technology; 2010.
[45] Swierczynski D, Courson C, Bedel L, Kiennemann A, Vilminot S. Oxidation reduction behavior of iron-bearing olivines $(Fe_xMg_{1-x})_2SiO_4$ used as catalysts for biomass gasification. Chem Mater 2006;18:897–905.
[46] Bennett L, Takacs L, Swartzendruber L, Weissmüller J, Bendersky L, Shapiro A. Magnetic properties of mechanically alloyed Fe-Ni-Ag. Scripta metallurgica materialia 1995;33:1717–24.
[47] Ejima T, Akasaka M, Ohfuji H. Oxidation state of Fe in olivine in a lherzolite xenolith from Oku district, Oki-Dogo Island, Shimane Prefecture, Japan. J Mineralogical Petrological Sci 2011;106:246–54.
[48] Shinno I. A Mössbauer study of ferric iron in olivine. Phys Chem Minerals 1981;7:91–5.
[49] Meyer M, Rüffler R. Conversion electron Mössbauer spectroscopic study of subsolidus oxidation of olivine. Hyperfine Interact 2002;141:351–5.
[50] Schaefer MW. Measurements of iron (III)-rich fayalites. Nature 1983;303:325–7.
[51] Michel R, Ammar MR, Poirier J, Simon P. Phase transformation characterization of olivine subjected to high temperature in air. Ceram Int 2013;39:5287–94.
[52] Hu C-W, Yao J, Yang H-Q, Chen Y, Tian A-M. On the inhomogeneity of low nickel loading methanation catalyst. J Catal 1997;166:1–7.
[53] Chang F-W, Hsiao T-J, Shih J-D. Hydrogenation of $CO_2$ over a rice husk ash supported nickel catalyst prepared by deposition-precipitation. Industrial Eng Chem Res 1998;37:3838–45.
[54] Garbarino G, Riani P, Magistri L, Busca G. A study of the methanation of carbon dioxide on Ni/$Al_2O_3$ catalysts at atmospheric pressure. Int J Hydrogen Energy 2014;39:11557–65.
[55] Takano H, Shinomiya H, Izumiya K, Kumagai N, Habazaki H, Hashimoto K. $CO_2$ methanation of Ni catalysts supported on tetragonal $ZrO_2$ doped with $Ca^{2+}$ and $Ni^{2+}$ ions. Int J Hydrogen Energy 2015;40:8347–55.
[56] Sehested J, Larsen KE, Kustov AL, Frey AM, Johannessen T, Bligaard T, et al. Discovery of technical methanation catalysts based on computational screening. Top Catal 2007;45:9–13.
[57] Guo M, Lu G. The difference of roles of alkaline-earth metal oxides on silica-supported nickel catalysts for $CO_2$ methanation. RSC Adv 2014;4:58171–7.
[58] Rostrup-Nielsen J, Pedersen K, Sehested J. High temperature methanation: sintering and structure sensitivity. Appl Catal A General 2007;330:134–8.
[59] Freire RM, de Sousa FF, Pinheiro AL, Longhinotti E, Mendes Filho J, Oliveira AC, et al. Studies of catalytic activity and coke deactivation of spinel oxides during ethylbenzene dehydrogenation. Appl Catal A General 2009;359:165–79.